Environment-friendly surface acoustic wave humidity sensor with sodium alginate sensing layer

Y.C. Han[a], W. Wu[a], X.Y. Kong[a], J.S. Li[b], X. Yang[b], Y.J. Guo[a,*], Y.Q. Fu[d], Hamdi Torun[d], X. Xiang[a], Y.L. Tang[c], X.T. Zu[a,*]

[a]School of Physics, University of Electronic Science and Technology of China, Chengdu, 610054, P. R. China

[b]Institute of Chemical materials, China Academy of Engineering Physics, Mianyang, 621900, P. R. China

[c]School of Physical Science and Technology, Southwest Jiaotong University, Chengdu, 610031, P. R. China

[d]Faculty of Engineering & Environment, University of Northumbria, Newcastle upon Tyne, NE1 8ST, UK

[*]Corresponding authors and E-mail addresses:

xtzu@uestc.edu.cn (X.T. Zu), guoyuanjun@uestc.edu.cn (Y.J. Guo)

Abstract:

A low-cost and environment-friendly surface acoustic wave (SAW) humidity sensor was fabricated on a quartz substrate using sol-gel/spin-coated sodium alginate (SA) sensing layer. The sensing mechanism is based on the frequency shift of the SAW sensor caused by both mass loading and electrical loading, with the former being the dominant factor. The SA film prepared in this study is an environment-friendly material with a large number of hydroxyl and carboxylate groups, which easily adsorb and react with H_2O molecules to form hydrogen bonds. These adsorbed H_2O molecules lead to significantly enhanced mass loading and signal responses of the SAW sensor. Electrical loading effect is also generated due to the transfer of hydrogen ions in the H_2O molecules, which alters the electrical resistance and results in changes of resonant frequencies of the SAW device. When the relative humidity (RH) is increased from 35% to 85%, the responses of the SAW sensor with 1 wt.% SA are significantly decreased. Whereas in a low humidity environment (e.g., RH <35%), the responses of the sensor show a linear relationship with the change of humidity. The developed humidity sensor shows good short-term/long-term stabilities and a low temperature coefficient of frequency.

Keywords: Surface acoustic wave, sensor; Sodium alginate (SA); Humidity

1. Introduction

Humidity monitoring is critical for various applications in food industries, agricultures, and electronics [1, 2]. Various humidity sensors have been developed including capacitive [3], resistive [4], quartz crystal microbalance-based [5, 6], optical [7] and surface acoustic wave (SAW) based ones [8, 9]. Most resistive and capacitive sensors require using conductive materials as the sensing layer, which limits the choice of materials for these sensors and temperature has often shown a great influence. Quartz crystal microbalance has a comparatively low sensitivity due to its low resonance frequency. Optical methods are often bulky and expensive [10, 11].

SAW-based humidity sensors have advantages, such as high sensitivity, small size, easy integration and low cost, with remote control and wireless functions [12, 13]. Most of the humidity sensors are based on the sensing mechanism of resistance changes of the sensing material, and there are a few reports of SAW-based humidity sensors. The sensing mechanism of a SAW humidity sensor is mainly based on the changes of mass of the sensitive film during the variation of RH values [19]. A conventional SAW sensor is a radio frequency (RF) oscillator consisting of a SAW resonator coated with a sensing layer and its corresponding amplification or phase shift circuits [14]. Different types of materials have been explored as the sensitive layer for SAW humidity sensors. For example, Su et al. [15] reported a SAW humidity sensor using a sensitive material of graphene/PVA/SiO_2, and the dynamic response of sensor was about 70 kHz with respect to a 70% change in the RH value. Lu et al. [16] demonstrated that SnO_2/MoS_2 can be used as a humidity sensing material, and the maximum responses can reach 62.4 kHz with respect to 80% change in the RH value. Despite the easiness of realizing humidity SAW resonators and oscillators, many of these sensitive materials are relatively expensive and sometimes difficult to synthesize, which greatly increases the cost of the fabricated humidity sensors. Therefore, it is critical to search a low-cost and environmentally friendly sensitive material for humidity sensing.

Sodium alginate (SA) is a by-product of the extraction of iodine and mannitol from

kelp or brown algae such as Sargassum. It is a natural polysaccharide, and its molecules are composed of β-D-mannouronic acid (M) and α-L-gulouronic acid (G) [17]. It can be obtained using simple and cost-effective processes, and it is insoluble in many organic solvents such as ethanol, ether, and chloroform. SA has been widely used in the field of medicine [18]. It is an environmentally friendly material and has a lot of hydroxyl and carboxylate groups, which are beneficial for humidity detection [19]. Hydroxyl and carboxylate groups in the SA film form hydrogen bonds with H_2O molecules [19]. In addition, they can also capture H_2O molecules through physical adsorption within its porous structure, thus enhancing the mass loading effect. Thus, the SA film can be applied as an excellent candidate of the sensing layer for the SAW-based humidity sensor. For example, Yun et al. [20] and Bian et al. [21] fabricated humidity sensors based on carbonized lignin/SA composite films and calcium alginate hydrogel films, respectively.

SA is an environmentally friendly biodegradable material with excellent hydrophilicity for humidity detection sensing, but it has never been reported as a sensitive material in SAW sensors. There are has two challenges using the SA as a sensing layer. Firstly, the concentration of the SA is a critical issue, because too large a concentration will cause the formation of a thick gel, thus causing the working issue of the SAW device. Secondly, the layer thick obtained using the spin coating will determine the detection performance of the device.

In this paper, SA was selected and optimized as the sensing film for SAW-based humidity sensor made on ST-cut quartz substrate owing to its nearly zero temperature coefficient of frequency (TCF). The sensor's humidity sensing performance and mechanisms were investigated systematically.

2. Experimental details

2.1. Fabrication of SAW resonator with SA sensing layer

Figure 1 illustrates the SAW resonator of the humidity sensor. It consists of a ST-

cut (42°75′) quartz substrate (12 mm × 3 mm × 0.5 mm), interdigital transducers (IDTs, aluminum layer with a thickness of 200 nm, 50 pairs), and reflective gratings (250 pairs). The aperture of the IDTs is 3 mm, and its wavelength is 16 microns. The SAW resonator's center frequency was designed to be 200 MHz.

SA (Macklin, ultra-low viscosity, and 1% viscosity) as the sensitive material was coated onto the SAW resonator using a sol-gel and spin coating process. Typically, SA powders of 1 g, 1.5 g, 2 g, 2.5 g were added into 99 mL, 98.5 ml, 98 ml, 97.5 ml deionized water, respectively, to prepare SA solutions using a magnetic stirrer at room temperature for 90 min. The obtained SA solutions were designated as 1 wt.%, 1.5 wt.%, 2 wt.%, 2.5 wt.%, respectively. They were kept for 24 hrs, and then ultrasonically agitated for 2 hrs. The prepared SA sols were spin-coated onto ST-cut quartz resonators at a speed of 300 rpm for 6 s and then at a high speed of 7000 rpm for 30 s. They were dried at 60^{o}C for 8 min to form a uniform SA film. The coating process was repeated on the sample surface to obtain SA layers with different thicknesses. The coated resonators were then dried for 12 hrs. Finally, the SAW resonators were connected to the oscillating circuits to form the SAW sensors.

2.2. Characterization of sensing platform

Fig. 2 schematically illustrate the experimental setup for humidity sensing. The temperature was kept at room temperature of 25^{O}C and the relative humidity (RH) was 35%. The SAW sensor was put inside a 20 L test chamber. The RH inside the test chamber was regulated by a digital humidity controller (GREE, SCK-40X71), and the RH values were adjusted to 45%, 55%, 65%, 75% and 85% by computer. The resonant frequency of the sensor was recorded using a frequency counter (Agilent 53210A), and the frequency shifts were measured as the responses of the sensor toward humidity.

A digital source-meter (Keithley 2400) was used to measure the conductivity of the sensor. Surface and cross-section morphologies of the SA film were characterized using a field-emission scanning electron microscope (FE-SEM, FEI Inspect F50). Surface functional groups of the SA film were characterized using a Fourier transform infrared spectroscope (FTIR, Nicolet IS 10, Thermo Fisher Scientific). Specific surface

area and porosity of the SA film were measured using a Brunauer–Emmett–Teller method with a nitrogen adsorption analyzer (Micromeritics, ASAP 2460).

3. Results and discussion

3.1 Film characterizations

Fig. 3 shows the SEM images of SA films. The thickness of one layer film is between 110 nm and 180 nm depending on different SA sol concentrations. As can be seen from Fig. 3, particulates appear on the surface of SA films with increasing SA concentration. This is mainly because with the increase of SA concentration, the SA becomes hard to be dissolved into water, and therefore, there are many particles remained in the solution.

Fig. 4(a) shows analysis results of functional groups of SA obtained using the FTIR. The absorption peak at 3447.92 cm^{-1} is the stretching vibration mode of O-H bonds [23-26]. The absorption peaks at 1631.99 cm^{-1} and 1410.13 cm^{-1} are the asymmetric $–COO^–$ stretching vibration and symmetric $–COO^–$ stretching vibration modes, respectively [26-28]. The absorption peak at 1033.53 cm^{-1} is linked to –C–O–C stretching vibration mode [23, 25, 26]. FTIR results clearly indicate that the SA has a large number of hydroxyl and carboxylic acid groups, which are crucial for the humidity sensing because these groups can form hydrogen bonds after reacting with H_2O molecules, as reported in refs. [1, 2, 19]. In addition, results from the BET and nitrogen adsorption analysis show that the specific surface area of SA is 0.49 m^2/g and the average pore diameter is 23.4 nm, as shown in Fig. 4(b). Figs. 4(a) and 4(b) clearly show that H_2O molecules are captured mainly by forming the hydrogen bonds with hydroxyl and carboxylic acid groups in the SA.

3.2 Humidity sensing results and mechanisms

As can be seen from Fig. 3, the films after two-layer coating process are thicker with minor delamination between the first and second layers. Fig. 5(a) shows the frequency shifts of 1 wt.% SA film with one and two coated layers when the RH is

increased from 35% to 65%. The frequency responses of two coated layers' film have not shown any significant increases compared with those of one coated layer's film. A similar phenomenon is also observed for the two layers of other concentrations' SA sols. This may be due to the delamination between the two layers, which makes it difficult for the H_2O molecules to enter the layer below. Therefore, a single coated layer of sensing film is selected in the following studies.

When the value of RH is increased from 35% to 65%, the frequency of sensors with one layer and four different concentrations of SA sols (1 wt.%, 1.5 wt.%, 2 wt.%, 2.5 wt.%) are found to decrease by 49.68 kHz, 26.71 kHz, 25.23 kHz and 24.87 kHz, respectively, as shown in Fig. 5(b). The differences in the frequency changes are mainly attributed to water vapor penetration rates, because the higher the SA concentration is, the denser the films and the lower porosities are, thus the lower water vapor penetration rate could be achieved [27, 29-31].

To determine if further decrease in the concentration of SA sol improves the sensor's performance, the frequency shifts of a single-layer SA film with 0.5 wt.% were measured, and the results are shown in Fig. 5(b). The frequency is only decreased by 11.84 kHz when the value of RH is increased from 35% to 65%. The decrease in the concentration of SA sol leads to a reduction in hydroxyl and carboxylic acid groups, thus resulting in a reduction in the frequency responses. Therefore, the single layer of 1 wt.% SA film was selected for the subsequent performance tests. Experiments with 50% RH change (e.g., from 35% RH to 85% RH) were carried out using the 1 wt.% SA film. Fig. 6 shows the sensors' dynamic responses to RH changes (e.g., from 35% RH to 85% RH).

Generally, the frequency changes of SAW sensors are affected by many factors, e.g., mass loading effect, electrical loading effect, elastic loading effect, and changes of temperature and pressure [1, 32, 33]. Because the experimental conditions were kept constants except the humidity, effects of temperature and pressure would not influence the performance of humidity sensing. Moreover, the adsorption of H_2O molecules did not apparently cause the SA film to become stiffer or softer. Therefore, mass loading effect and electrical loading effect are the two main factors affecting the sensor's

performance.

The changes in the electrical resistance are mainly caused by the transfer of protons among H_2O molecules. Hydrogen ions and hydroxide ions are transferred among different water molecules. The charges are transported when the H_2O molecules transfer protons to a neighboring H_2O molecule and forms the H_3O^+, as shown in formula (1). The hydrogen ions (protons) are transferred from one water vapor molecule to another, thereby leading to a remarkable change of electrical resistance [19].

$$H_2O + H_2O \Leftrightarrow H_3O^+ + OH^- \quad (1)$$

The change of the conductivity of the sensitive film will change the velocity of the SAW device, thus leading to a frequency shift of the SAW sensor. The relationship between the frequency shifts (Δf) versus the surface conductivity (σ_s) of the film can be described as follows [34]:

$$\frac{\Delta f}{f_0} = \frac{\Delta v}{v_0} \approx \frac{-K^2}{2} \frac{\sigma_s^2}{\sigma_s^2 + v_0^2 C_s^2} \quad (2)$$

where f_0 is the central frequency of the SAW device (e.g., 200 MHz); $v_0 = 3158$ m/s is the theoretical SAW velocity on the ST-cut quartz surface. K^2=0.11% is the electromechanical coupling coefficient. $C_s = 0.5$ pF/cm is the capacity per unit length, which is the sum of the air dielectric constant and the substrate dielectric constant, $\sigma_s = h/\rho$ (ρ is the resistivity and h is the thickness of the films). ξ is defined as the acoustoelectric parameter, i.e., $\xi = \frac{\sigma_s}{v_0 C_s}$. The relationship between ξ and Δf is shown in Fig. 7(a), in which the data points represent the values of ξ under different RH values. For one layer film, if ξ is between 0.1 and 10, there is a significant frequency shift [34].

When the RH value is increased from 35% RH to 85% RH, the electrical loading effect causes significant frequency shifts. Fig. 7(b) shows the resistance changes when the RH is changed from 35% RH to 85% RH. R_0 is the dynamic resistance value at

35% RH, and R_f is the dynamic resistance value at 85% RH. The peak value of R_0 / R_f obtained from Figure 7(b) is around 1100. The Δf value calculated using the formula (2) is -32.64 kHz. All the calculated frequency shifts under different RH changes are summarized in Table 1. Results show that the larger the humidity change, the greater the influence of the electrical loading effect is on the frequency responses. Although the electrical loading effect shows its increased effect on the frequency responses when the RH changes are above 30%, it contributes only a small portion of the total frequency responses, as seen from Table 1. Therefore, the mass loading effect should be the main reason for the negative frequency shift of SAW humidity sensor.

The adsorbed water molecules due to humidity lead to an increase in the weight of the film, which causes the negative response as follows [35]:

$$\Delta f = (\kappa_1 + \kappa_2) f_0 \Delta m \tag{3}$$

where $\kappa_1 = -8.7 \times 10^{-8} \mathrm{m^2 s/kg}$ and $\kappa_2 = -3.9 \times 10^{-8} \mathrm{m^2 s/kg}$ are the matrix constants of the ST-cut quartz. As shown in Formula (3), since both κ_1 and κ_2 are negative values, an increase in the mass loading will cause a negative shift of Δf.

Results of BET and nitrogen adsorption analysis show that SA has a poor ability to physically adsorb H_2O molecules due to its small pore size. Therefore, most of the H_2O molecules are captured by forming hydrogen bonds with hydroxyl and carboxylic acid groups. Fig. 8(a) illustrates the structure of SA [17, 24]. Fig 8(b) shows the process in which hydroxyl and carboxylate groups combine with water molecules to form hydrogen bonds. The hydrogen ions of the hydroxyl group in SA form hydrogen bonds with the oxygen atom in the H_2O molecule, and the hydrogen ions in one H_2O molecule can form hydrogen bonds with the oxygen atoms in the other H_2O molecule. Therefore, more H_2O molecules are concentrated on the surface of SA film, resulting in an increase in mass loading of SA film. In addition, the carboxylate ions can also form hydrogen bonds with the hydrogen atoms of H_2O molecules, which increases the mass loading effect of SA film, as shown in Fig. 8(b).

Fig. 9(a) shows the dynamic responses of SAW sensor with 1 wt.% SA film when

the humidity level is increased to 10% RH, 20% RH, 30% RH, 40% RH and 50% RH, respectively, from the initial humidity of 35% RH at room temperature. The average frequencies of the SAW sensor under five different RH conditions are decreased by 9.443 kHz, 29.125 kHz, 49.683 kHz, 60.807 kHz and 102.2 kHz, respectively. Fig. 9(b) shows that the frequency shifts are decreased in an exponential function with the RH level changed from 35% to 85%. The reason is that under a high RH value (above 75% RH), water condensation occurs due to the formation of hydrogen bonds, which causes a significantly negative frequency shift of the SAW sensor [2, 19].

Meanwhile, sensing precision at lower humidity levels (e.g., from 5% RH to ~35% RH) is also important for humidity sensors. We have applied high-purity and dry argon gas to be injected into the test chamber during humidity sensing tests in order to change the humidity, effectively. The results of frequency shifts are shown in Fig. 9(c). A linear fitting is conducted for the obtained data as shown in Fig. 9(c), and the obtained R^2 value is 0.998, which shows an excellent linearity as a function of the value of RH under low humidity levels (e.g., 5% RH-35% RH).

The TCF value of the device was further obtained to assess the thermal stability of the SAW device, based on the following definition:

$$|\mathrm{TCF}|=\left|\frac{1}{f_0}\cdot\frac{\Delta f}{\Delta T}\right| \tag{4}$$

where f_0 is the central frequency of the SAW device (which is 200 MHz); Δf is the change in frequency, and ΔT is the change in temperature. In the experiment, the ST-cut quartz substrate was heated by a heating device (JFTOOIS, V-1010, 100 mm x 100 mm), and the temperature was increased from 25℃ to 60℃. Fig. 10(a) shows that there is a good linear relationship between temperature and frequency shift, and the TCF value is 0.14 ppm/℃. Compared with the SAW devices on other substrates summarized in the Table 2, the stability of ST-Cut quartz SAW device is excellent.

The short-term stability and long-term stability of SAW sensor were further evaluated with the humidity level changed from 35% RH to 65% RH. As shown in Fig. 10(b), the dynamic response of the sensor is nearly the same (with a maximum value

of 2.9 kHz) for the six RH changing cycles, indicating that the SAW sensor based on the SA film has a good short-term stability. Fig. 10(c) shows the obtained sensing results when the SAW sensors coated with the SA film were kept inside the test chamber with 35% RH, 45% RH, 55% RH, 65% RH, 75% RH, and 85% RH for 75 days. The dynamic responses of the sensor are slightly decreased (about 5000 Hz) for all different humidity levels, which is caused by the natural decomposition of organic matter and the solubility of SA in water. Nevertheless, the frequency changes of the SAW humidity sensor based on the SA film is less than 1% for each humidity environment over 75 days. Therefore, the SAW humidity sensor based on SA film has shown a good long-term stability.

Finally, we compared the frequency shifts of this sensor with those of the humidity sensors reported in the literature, and the comparisons are listed in Table 3. Among the reported SAW humidity sensors, the SA coated SAW humidity sensor offers good combination of performance, cost, and convenience. In comparison, most of the high-performance humidity sensors have either a high production cost or a complex preparation process, which are difficult for practical applications. Therefore, SA is a relatively good material for humidity sensing application due to its good detection performance, low cost, and environment-friendliness.

4. Conclusions

In this paper, a low-cost surface acoustic wave (SAW) humidity sensor with a good performance based on sodium alginate (SA) film was fabricated. Comparisons of SEM images and frequency responses showed that a single-layer of SA film is optimum for this SAW humidity sensor. By comparing the performance of SA solution at different concentrations under the same humidity change, the best SA solution concentration is determined to be 1 wt.%. The dynamic response of the SA SAW humidity sensor is increased with increasing the humidity. Regarding to the humidity sensing mechanisms, the mass loading and electrical loading effects contribute to the negative frequency shifts of SAW humidity sensor, where the dominant factor is the mass loading effect.

The presence of a large number of hydroxyl groups in SA structure and the formation of intermolecular hydrogen bonds with H_2O molecules are regarded as the key mechanisms for the humidity sensing. The frequency response tends to increase exponentially with the increase of RH values. However, in a low humidity environment (e.g., 5%RH-35%RH), the SA SAW humidity sensor exhibits an excellent linearity to the changes in RH. The SA SAW humidity sensor also show both good long-term and short-term stability.

Acknowledgments

This study was supported financially by the Joint Fund of the National Natural Science Foundation of China and the China Academy of Engineering Physics (Grant No. U1930205), Engineering Physics and Science Research Council of UK (EPSRC EP/P018998/1) , and International Exchange Grant (IEC/NSFC/201078) through Royal Society and the National Natural Science Foundation of China (NSFC), and Royal Academy of Engineering: Research Exchange between UK and China.

References

[1] Tang, Y.; Li, Z.; Ma, J.; Wang, L.; Yang, J.; Du, B.; Yu, Q.; Zu, X., Highly sensitive surface acoustic wave (SAW) humidity sensors based on sol-gel SiO_2 films: Investigations on the sensing property and mechanism. *Sensors and Actuators B-Chemical* **2015,** *215*, 283-291.

[2] Wang, J. L.; Guo, Y. J.; Li, D. J.; Long, G. D.; Tang, Q. B.; Zu, X. T.; Ma, J. Y.; Du, B.; Tang, Y. L.; Torun, H.; Fu, Y. Q., Bacterial cellulose coated ST-cut quartz surface acoustic wave humidity sensor with high sensitivity, fast response and recovery. *Smart Materials and Structures* **2020,** *29* (4), 1-11.

[3] Hong, H. P.; Jung, K. H.; Kim, J. H.; Kwon, K. H.; Lee, C. J.; Yun, K. N.; Min, N. K., Percolated pore networks of oxygen plasma-activated multi-walled carbon nanotubes for fast response, high sensitivity capacitive humidity sensors. *Nanotechnology* **2013,** *24* (8), 1-9.

[4] Tang, Q.-Y.; Chan, Y. C.; Zhang, K., Fast response resistive humidity sensitivity of polyimide/multiwall carbon nanotube composite films. *Sensors and Actuators B-Chemical* **2011,** *152* (1), 99-106.

[5] Zheng, X.; Fan, R.; Li, C.; Yang, X.; Li, H.; Lin, J.; Zhou, X.; Lv, R., A fast-response and highly linear humidity sensor based on quartz crystal microbalance. *Sensors and Actuators B-Chemical* **2019,** *283*, 659-665.

[6] Neshkova, M.; Petrova, R.; Petrov, V., Piezoelectric quartz crystal humidity sensor using chemically modified nitrated polystyrene as water sorbing coating. Analytica Chimica Acta 1996, 332 (1), 93-103.

[7] Voznesenskiy, S. S.;Sergeev,A. A.; Mironenko, A. Y.; Bratskaya, S. Y.; Kulchin, Y. N., Integrated-optical sensors based on chitosan waveguide films for relative humidity measurements. Sensors and Actuators B: Chemical 2013, 188, 482-487.

[8] Rimeika, R.; Ciplys, D.; Poderys, V.; Rotomskis, R.; Balakauskas, S.; Shur, M. S., Subsecond-response SAW humidity sensor with porphyrin nanostructure deposited on bare and metallised piezoelectric substrate. Electronics Letters 2007, 43 (19), 1055-1057.

[9] Rimeika, R.; Ciplys, D.; Poderys, V.; Rotomskis, R.; Shur, M. S.; Ieee In Humidity Sensor using Leaky Surface Acoustic Waves in YX-LiTaO3 with Nanostructured Porphyrin Film, 8th IEEE Conference on Sensors, Christchurch, NEW ZEALAND, Oct 25-28; Christchurch, NEW ZEALAND, 2009; pp 1753-+.

[10] Rao, X.; Zhao, L.; Xu, L.; Wang, Y.; Liu, K.; Wang, Y.; Chen, G. Y.; Liu, T.; Wang, Y., Review of Optical Humidity Sensors. 2021, 21 (23), 8049.

[11] Chen, G. Y.; Lancaster, D. G.; Monro, T. M., Optical Microfiber Technology for Current, Temperature, Acceleration, Acoustic, Humidity and Ultraviolet Light Sensing. Sensors 2018, 18 (1).

[12] Huang, P. H., Sensor calibration of a SAW resonator for absolute humidity measurements in microelectronic packages. Sensors and Actuators B-Chemical 1995, 25 (1-3), 686-688.

[13] Penza, M.; Anisimkin, V. I., Surface acoustic wave humidity sensor using polyvinyl-alcohol film. Sensors and Actuators a-Physical 1999, 76 (1-3), 162-166.
[14] Wen, W.; He, S.; Li, S.; Liu, M.; Yong, P., Enhanced sensitivity of SAW gas sensor coated molecularly imprinted polymer incorporating high frequency stability oscillator. *Sensors and Actuators B-Chemical* **2007,** *125* (2), 422-427.
[15] Su, Y.; Li, C.; Li, M.; Li, H.; Xu, S.; Qian, L.; Yang, B., Surface acoustic wave humidity sensor based on three-dimensional architecture graphene/PVA/SiO_2 and its application for respiration monitoring. *Sensors and Actuators B-Chemical* **2020,** *308,1-11*.
[16] Lu, L.; Liu, J.; Li, Q.; Yi, Z.; Liu, J.; Wang, X.; Chen, X.; Yang, B., High Performance SnO_2/MoS_2-Based Surface Acoustic Wave Humidity Sensor With Good Linearity. *Ieee Sensors Journal* **2019,** *19* (23), 11027-11033.
[17] Liu, S.; Li, Y.; Li, L., Enhanced stability and mechanical strength of sodium alginate composite films. *Carbohydrate Polymers* **2017,** *160*, 62-70.
[18] Gazori, T.; Khoshayand, M. R.; Azizi, E.; Yazdizade, P.; Nomanie, A.; Haririan, I., Evaluation of Alginate/Chitosan nanoparticles as antisense delivery vector: Formulation, optimization and in vitro characterization. *Carbohydrate Polymers* **2009,** *77* (3), 599-606.
[19] Farahani, H.; Wagiran, R.; Hamidon, M. N., Humidity Sensors Principle, Mechanism, and Fabrication Technologies: A Comprehensive Review. *Sensors* **2014,** *14* (5), 7881-7939.
[20] Yun, X.; Zhang, Q.; Luo, B.; Jiang, H.; Chen, C.; Wang, S.; Min, D., Fabricating Flexibly Resistive Humidity Sensors with Ultra-high Sensitivity Using Carbonized Lignin and Sodium Alginate. *Electroanalysis* **2020,** *32* (10), 2282-2289.
[21] Bian, C.; Cheng, Y.; Zhu, W.; Tong, R.; Hu, M.; Gang, T., A Novel Optical Fiber Mach-Zehnder Interferometer Based on the Calcium Alginate Hydrogel Film for Humidity Sensing. *Ieee Sensors Journal* **2020,** *20* (11), 5759-5765.
[22] Le, X.; Liu, Y.; Peng, L.; Pang, J.; Xu, Z.; Gao, C.; Xie, J., Surface acoustic wave humidity sensors based on uniform and thickness controllable graphene oxide thin films formed by surface tension. *Microsystems & Nanoengineering* **2019,** *5,1-10*.
[23] Bajpai, S. K.; Bajpai, M.; Shah, F. F., Alginate dialdehyde (AD)-crosslinked casein films: synthesis, characterization and water absorption behavior. *Designed Monomers and Polymers* **2016,** *19* (5), 406-419.
[24] Khalid, I.; Ahmad, M.; Minhas, M. U.; Barkat, K., Preparation and characterization of alginate-PVA-based semi-IPN: controlled release pH-responsive composites. *Polymer Bulletin* **2018,** *75* (3), 1075-1099.
[25] Peng, L.; Liu, Y.; Huang, J.; Li, J.; Gong, J.; Ma, J., Microfluidic fabrication of highly stretchable and fast electro-responsive graphene oxide/polyacrylamide/alginate hydrogel fibers. *European Polymer Journal* **2018,** *103*, 335-341.
[26] Abd El-Ghaffar, M. A.; Hashem, M. S.; El-Awady, M. K.; Rabie, A. M., pH-sensitive sodium alginate hydrogels for riboflavin controlled release. *Carbohydrate Polymers* **2012,** *89* (2), 667-675.
[27] Caykara, T.; Demirci, S.; Eroglu, M. S.; Guven, O., Poly(ethylene oxide) and its blends with sodium alginate. *Polymer* **2005,** *46* (24), 10750-10757.

[28] Hirai, A.; Odani, H., Sorption and transport of water-vapor in alginic acid, sodium alginate, and alginate-cobalt complex films. *Journal of Polymer Science Part B-Polymer Physics* **1994,** *32* (14), 2329-2337.
[29] Rhim, J. W., Physical and mechanical properties of water resistant sodium alginate films. *Lebensmittel-Wissenschaft Und-Technologie-Food Science and Technology* **2004,** *37* (3), 323-330.
[30] Yang, L.; Yang, J.; Qin, X.; Kan, J.; Zeng, F.; Zhong, J., Ternary composite films with simultaneously enhanced strength and ductility: Effects of sodium alginate-gelatin weight ratio and graphene oxide content. *International Journal of Biological Macromolecules* **2020,** *156*, 494-503.
[31] Yang, M.; Xia, Y., Preparation and characterization of nano-SiO_2 reinforced alginate-based nanocomposite films (II). *Journal of Applied Polymer Science* **2017,** *134* (38), 1-9.
[32] Borrero, G. A.; Bravo, J. P.; Mora, S. F.; Velasquez, S.; Segura-Quijano, F. E., Design and fabrication of SAW pressure, temperature and impedance sensors using novel multiphysics simulation models. *Sensors and Actuators a-Physical* **2013,** *203*, 204-214.
[33] Raja, V. B.; Nimal, A. T.; Parmar, Y.; Sharma, M. U.; Gupta, V., Investigations on the origin of mass and elastic loading in the time varying distinct response of ZnO SAW ammonia sensor. *Sensors and Actuators B-Chemical* **2012,** *166*, 576-585.
[34] Jakubik, W., Elemental theory of a SAW gas sensor based on electrical conductivity changes in bi-layer nanostructures. *Sensors and Actuators B-Chemical* **2014,** *203*, 511-516.
[35] Cheeke, J. D. N.; Wang, Z., Acoustic wave gas sensors. *Sensors and Actuators B-Chemical* **1999,** *59* (2-3), 146-153.
[36] He, X. L.; Li, D. J.; Zhou, J.; Wang, W. B.; Xuan, W. P.; Dong, S. R.; Jin, H.; Luo, J. K., High sensitivity humidity sensors using flexible surface acoustic wave devices made on nanocrystalline ZnO/polyimide substrates. *Journal of Materials Chemistry C* **2013,** *1* (39), 6210-6215.
[37] Le Brizoual, L.; Sarry, F.; Elmazria, O.; Alnot, P.; Ballandras, S.; Pastureaud, T., GHz frequency ZnO/Si SAW device. *Ieee Transactions on Ultrasonics Ferroelectrics and Frequency Control* **2008,** *55* (2), 442-450.
[38] Du, X. Y.; Swanwick, M. E.; Fu, Y. Q.; Luo, J. K.; Flewitt, A. J.; Lee, D. S.; Maeng, S.; Milne, W. I., Surface acoustic wave induced streaming and pumping in 128 degrees Y-cut $LiNbO_3$ for microfluidic applications. *Journal of Micromechanics and Microengineering* **2009,** *19* (3), 1-10.
[39] Mittal, U.; Islam, T.; Nimal, A. T.; Sharma, M. U., A Novel Sol-Gel gamma-Al2O3 Thin-Film-Based Rapid SAW Humidity Sensor. *Ieee Transactions on Electron Devices* **2015,** *62* (12), 4236-4244.
[40] Xu, Z.; Li, Z., Design and Fabrication of ZnO-Based SAW Sensor Using Low Power Homo-Buffer Layer for Enhanced Humidity Sensing. *Ieee Sensors Journal* **2021,** *21* (6), 7428-7433.
[41] Wu, T.-T.; Chen, Y.-Y.; Chou, T.-H., A high sensitivity nanomaterial based SAW humidity sensor. *Journal of Physics D-Applied Physics* **2008,** *41* (8), 1-3.

[42] Alam, S.; Islam, T.; Mittal, U., A Sensitive Inexpensive SAW Sensor for Wide Range Humidity Measurement. *Ieee Sensors Journal* **2020,** *20* (1), 546-551.
[43] Hong, H.-S.; Phan, D.-T.; Chung, G.-S., High-sensitivity humidity sensors with ZnO nanorods based two-port surface acoustic wave delay line. *Sensors and Actuators B-Chemical* **2012,** *171*, 1283-1287.
[44] Le, X.; Wang, X.; Pang, J.; Liu, Y.; Fang, B.; Xu, Z.; Gao, C.; Xu, Y.; Xie, J., A high performance humidity sensor based on surface acoustic wave and graphene oxide on A1N/Si layered structure. *Sensors and Actuators B-Chemical* **2018,** *255*, 2454-2461.

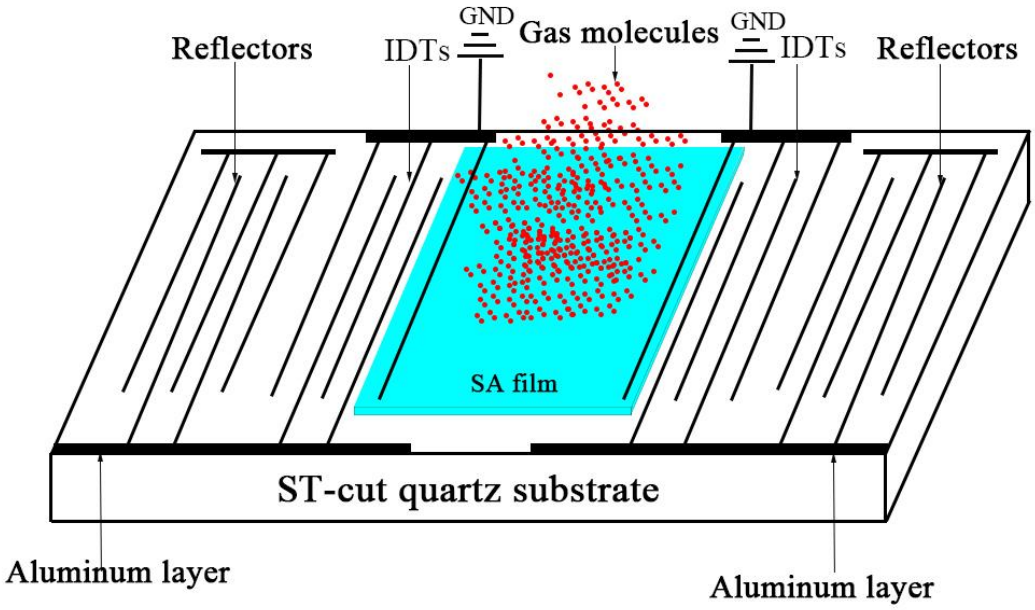

Fig. 1. Schematic illustration of SAW resonator

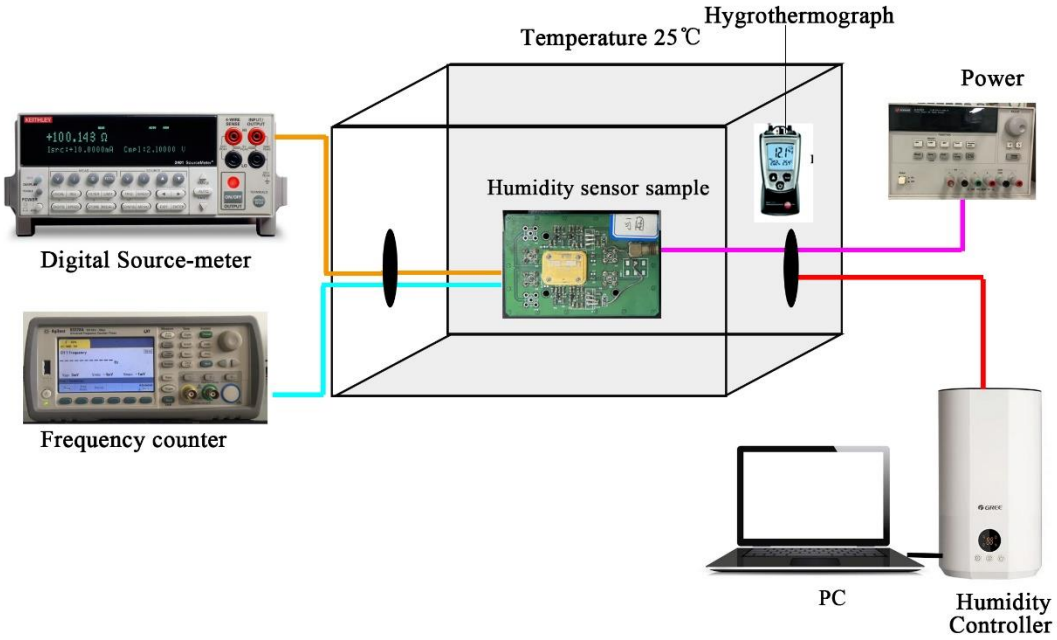

Fig. 2. Schematic diagram of experimental setup for humidity measurement.

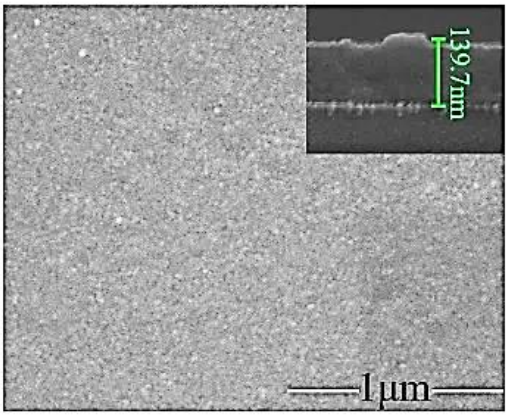

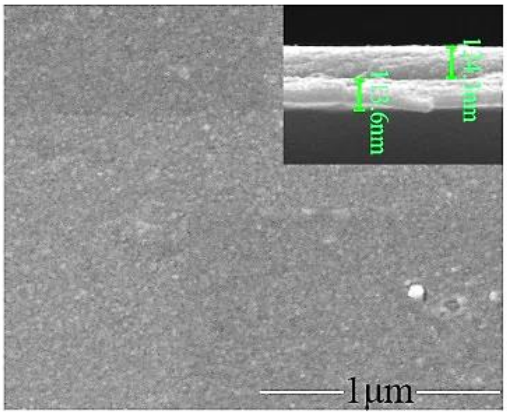

(a)

(b)

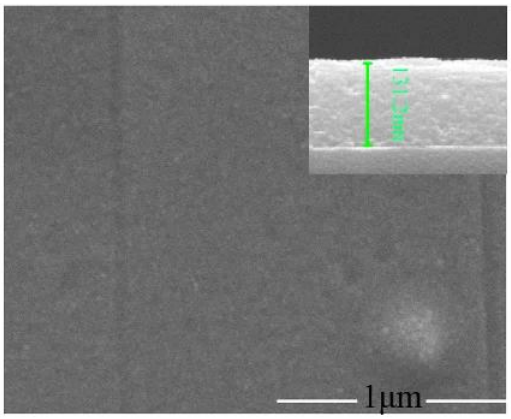

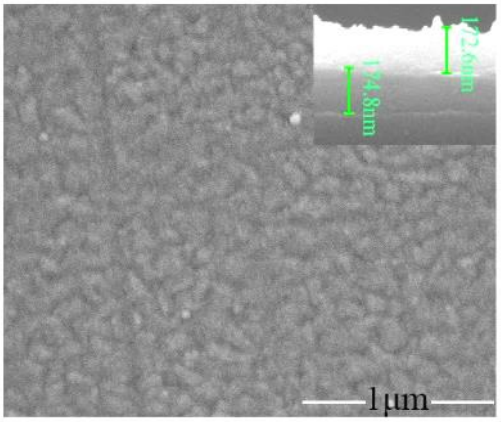

(c)

(d)

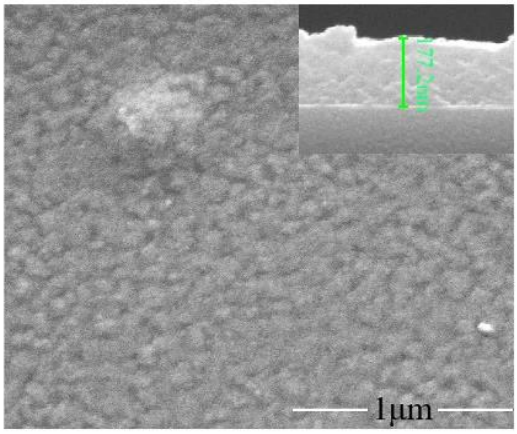

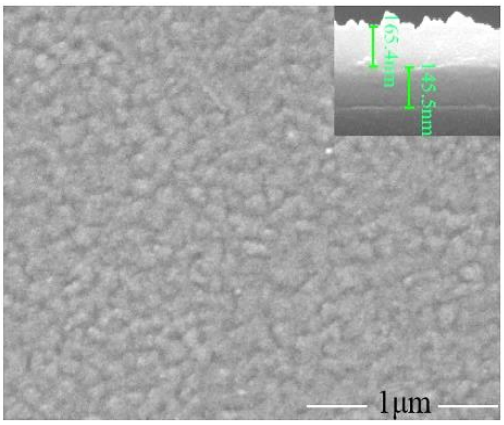

(e)

(f)

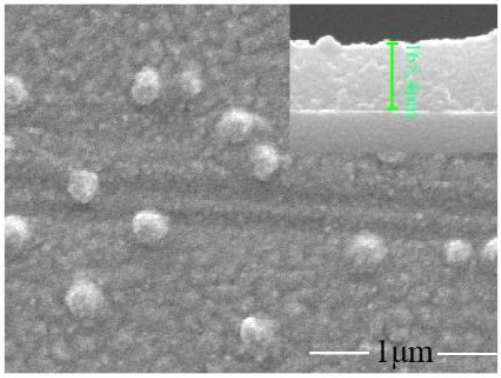

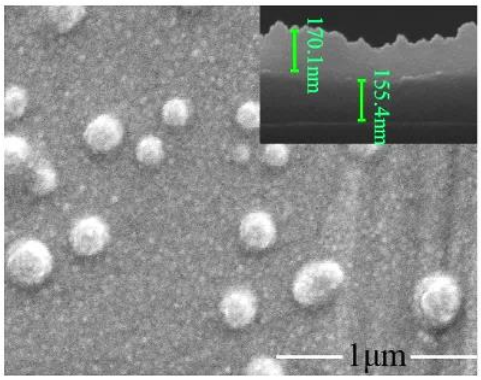

(g) (h)

Fig.3. SEM images of surface and cross-section morphologies (inset) of SA films with different layers and concentrations : (a) one layer, 1 wt%; (c) one layer, 1.5 wt%; (e) one layer, 2 wt%; (g) one layer, 2.5 wt%; (b) two layers, 1 wt%;, (d) two layers, 1.5 wt%;, (f) two layers, 2 wt%; (h) two layers, 2.5 wt%.

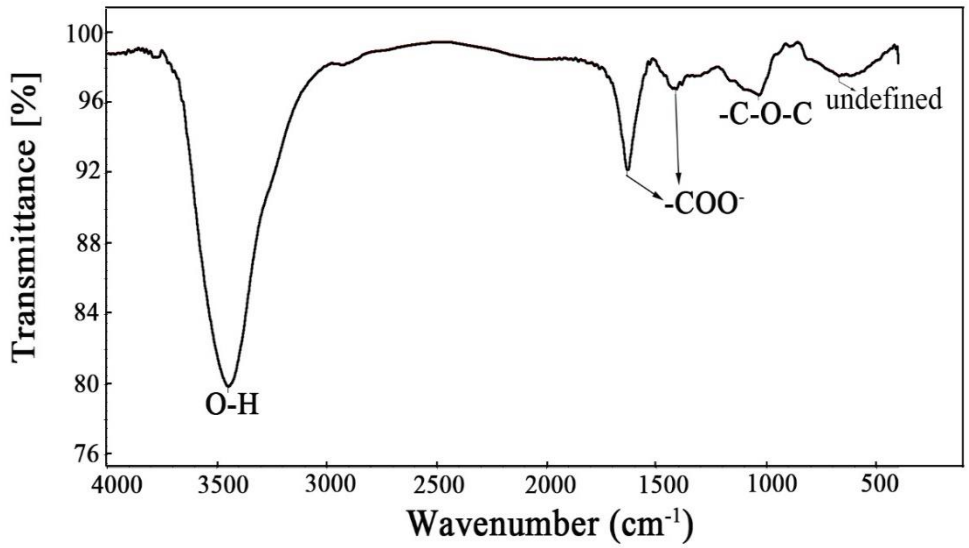

(a)

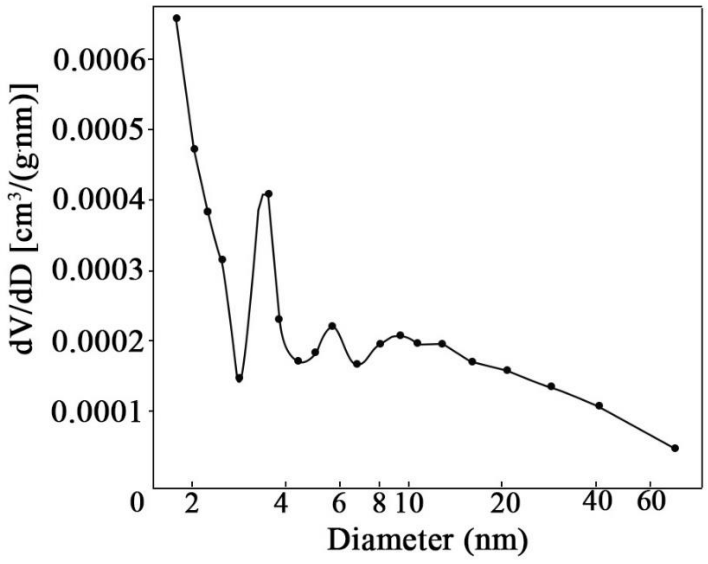

(b)

Fig.4. (a) FTIR spectrum of SA; (b) pore size distribution of SA

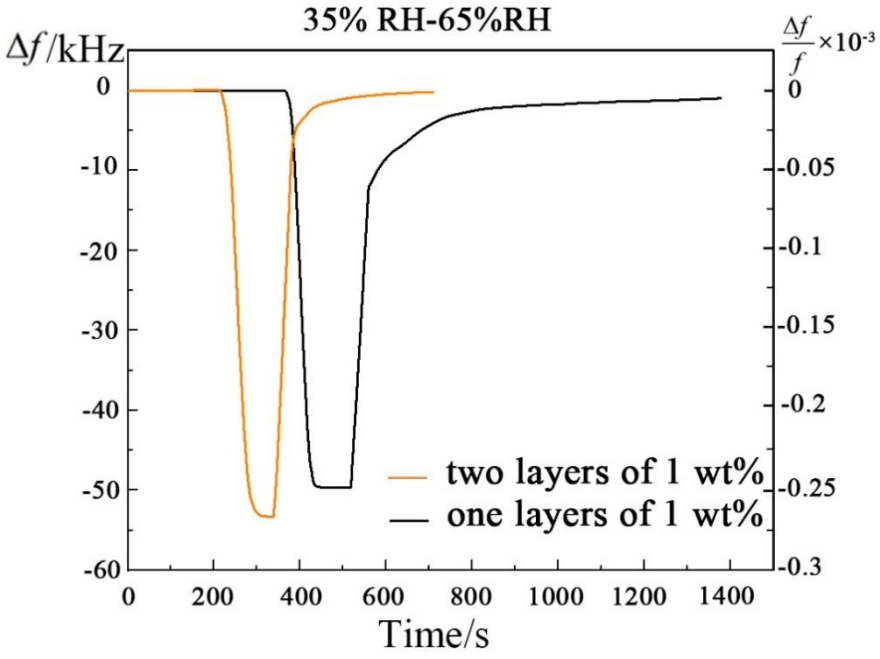
35% RH-65%RH
Δf/kHz
Δf/f ×10⁻³
0
-10
-20
-30
-40
-50
-60
0
-0.05
-0.1
-0.15
-0.2
-0.25
-0.3
0
200
400
600
800
1000
1200
1400
Time/s
two layers of 1 wt%
one layers of 1 wt%

(a)

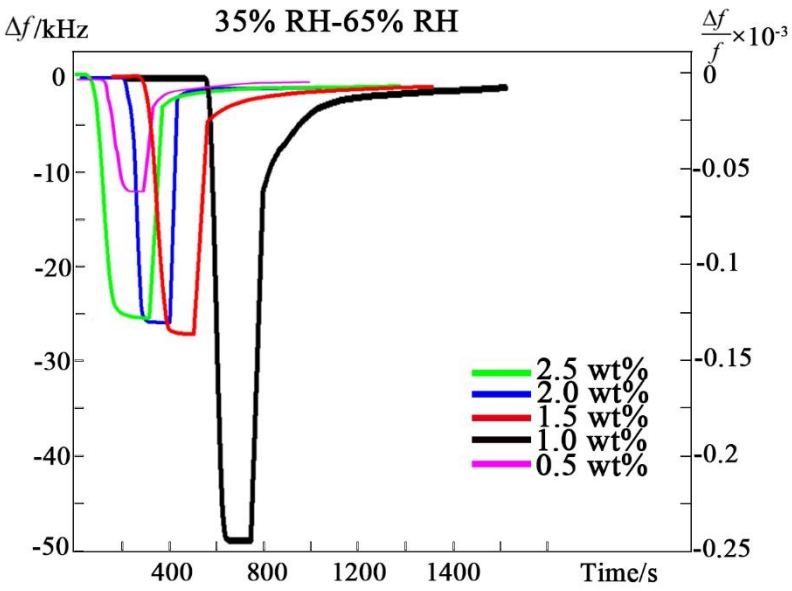

(b)

Fig.5. (a) Frequency shifts of 1 wt% SA film with one and two layers when RH is increased from 35% to 65%; (b) Frequency shifts of one layer SA film with different concentrations (0.5 wt%, 1 wt%, 1.5 wt%, 2 wt% and 2.5 wt%) when RH is increased from 35% to 65%.

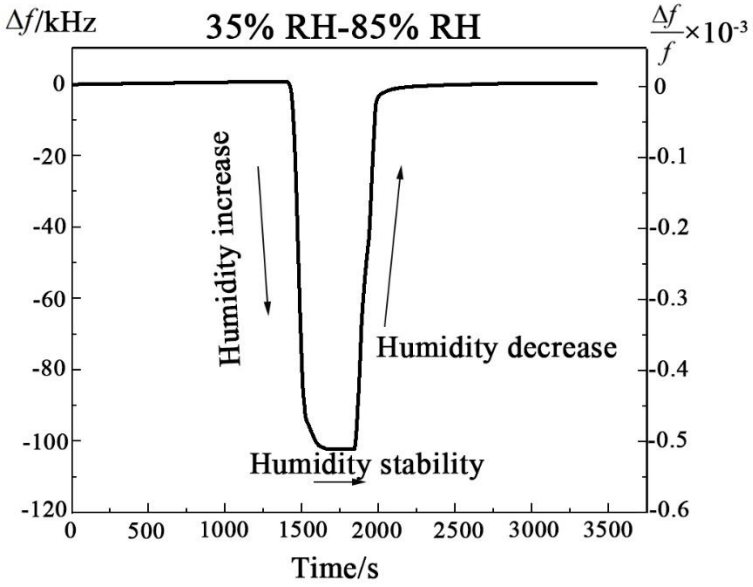

Fig.6. Frequency shifts of SAW devices when the RH values changed from 35% RH to 85% RH

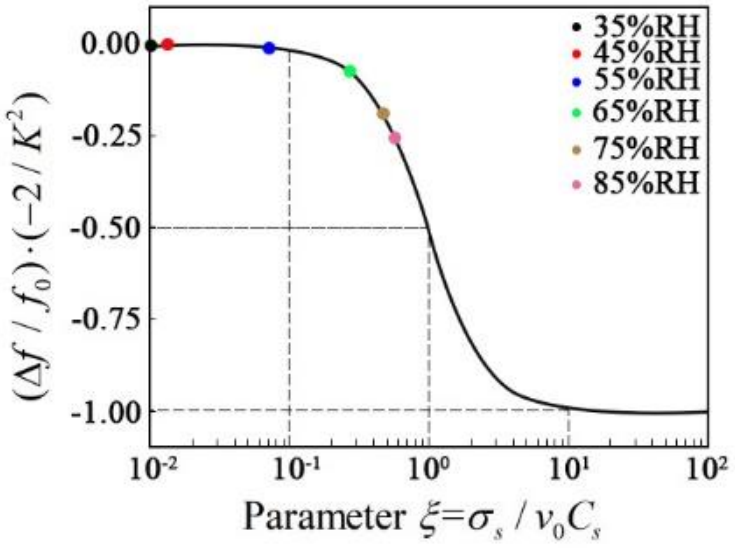

(a)

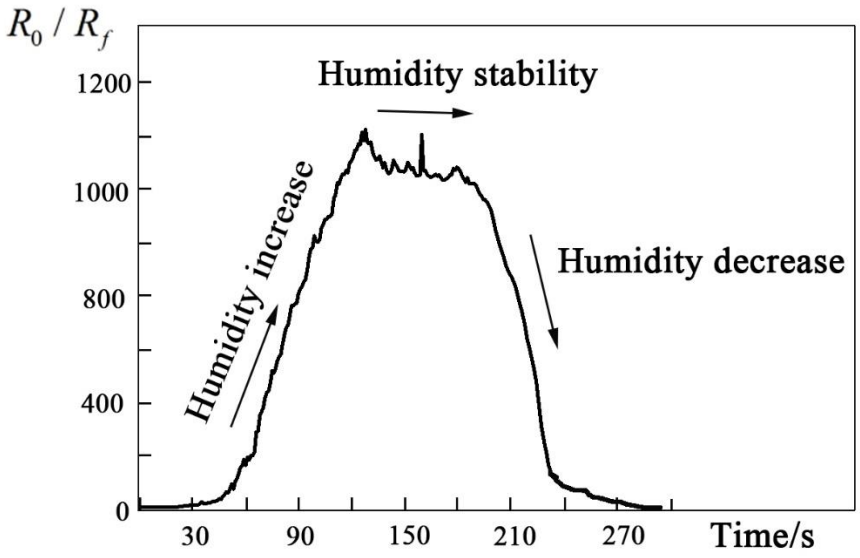

(b)

Fig.7. (a) Frequency changes of SAW sensor versus acoustoelectric parameter ξ;

(b) SA film resistance changes when humidity changes between 35%RH and 85%RH

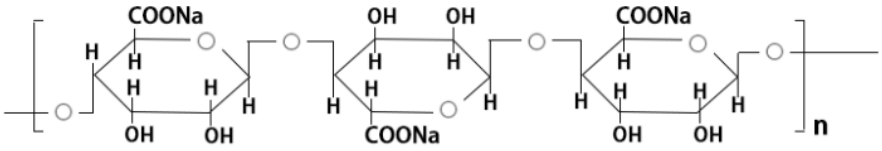

(a)

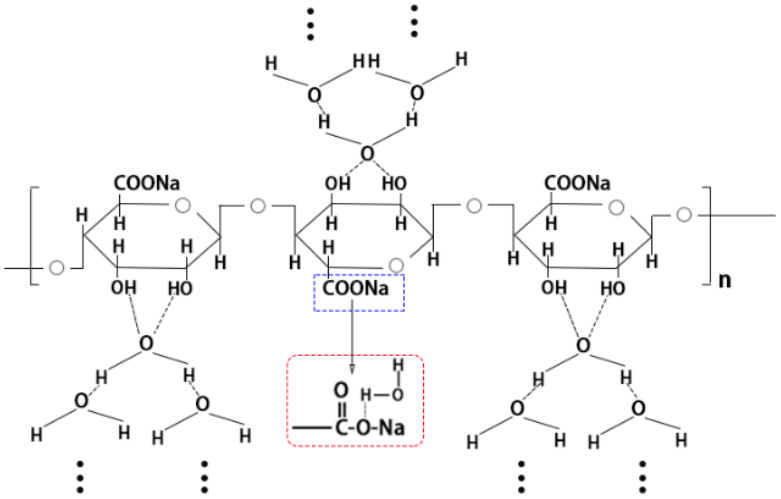

(b)

Fig.8 (a) Illustration of structures of SA; (b) The process for the hydroxyl groups and carboxylate to combine with water molecules, forming hydrogen bonds.

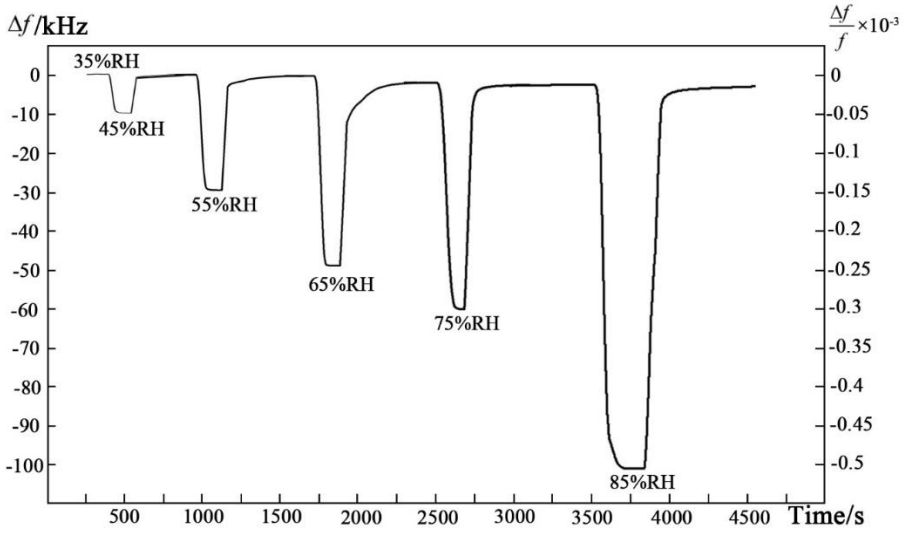
Δf/kHz
Δf/f ×10⁻³
35%RH
45%RH
55%RH
65%RH
75%RH
85%RH
0
-10
-20
-30
-40
-50
-60
-70
-80
-90
-100
0
-0.05
-0.1
-0.15
-0.2
-0.25
-0.3
-0.35
-0.4
-0.45
-0.5
500
1000
1500
2000
2500
3000
3500
4000
4500
Time/s

(a)

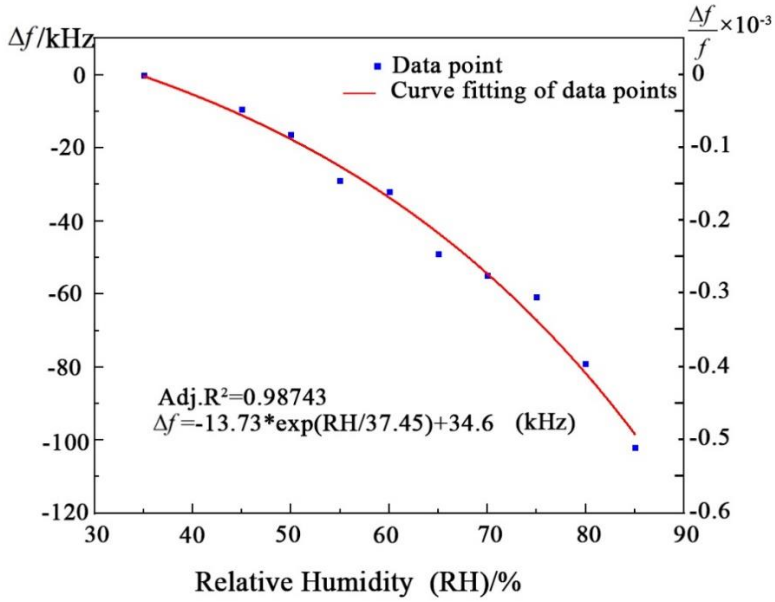
Δf/kHz
Δf/f ×10⁻³
Data point
Curve fitting of data points
Adj.R²=0.98743
Δf=-13.73*exp(RH/37.45)+34.6 (kHz)
0
-20
-40
-60
-80
-100
-120
0
-0.1
-0.2
-0.3
-0.4
-0.5
-0.6
30
40
50
60
70
80
90
Relative Humidity (RH)/%

(b)

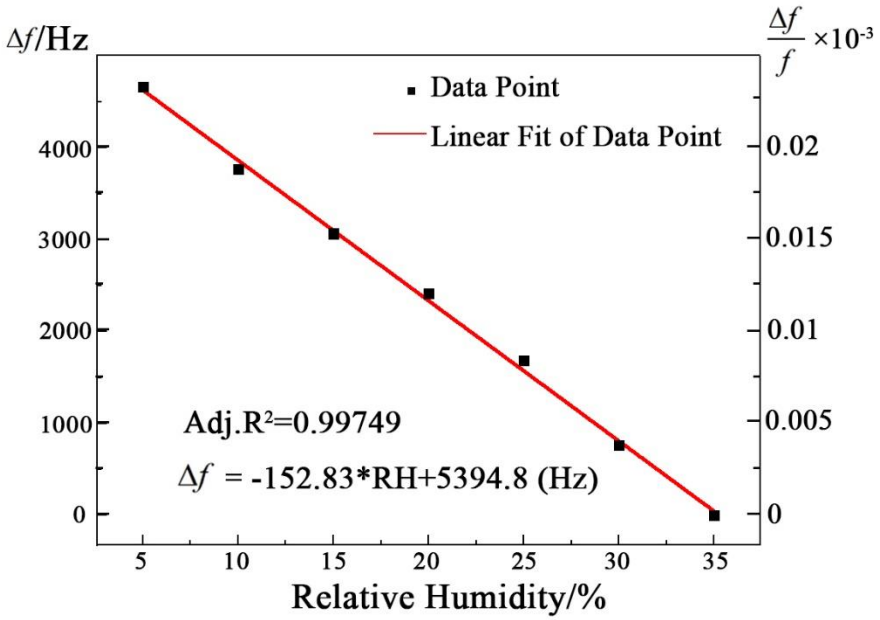

(c)

Fig.9 (a) Dynamic responses of the SAW sensor when the RH is changed from 35%RH to 45%RH, 55%RH, 65%RH, 75%RH, 85%RH, respectively; (b) the relationship between the frequency shifts of SAW sensor and RH (from 35% to 85%); (c) the relationship between the frequency shifts of the SAW sensor and RH in a low humidity environment (5%RH-35%RH)

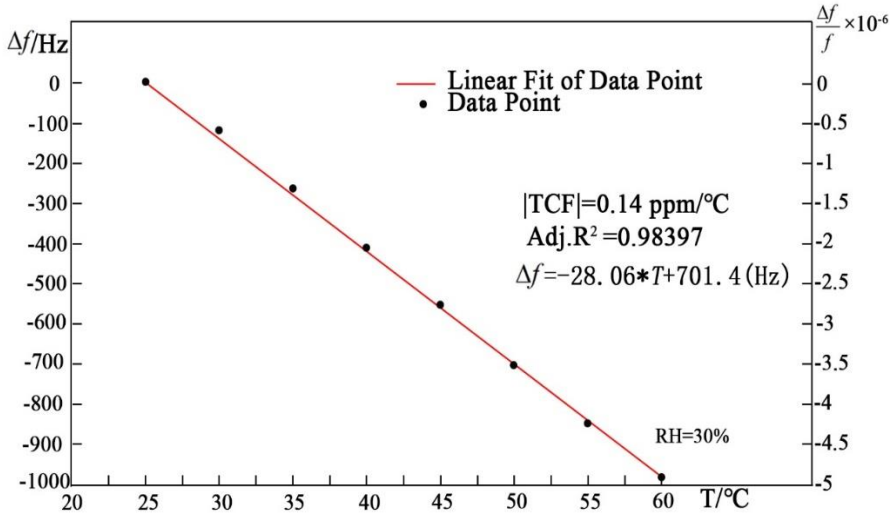
Δf/Hz
Δf/f ×10⁻⁶
Linear Fit of Data Point
Data Point
|TCF|=0.14 ppm/℃
Adj.R² =0.98397
Δf=−28. 06∗T+701. 4 (Hz)
RH=30%
T/℃

(a)

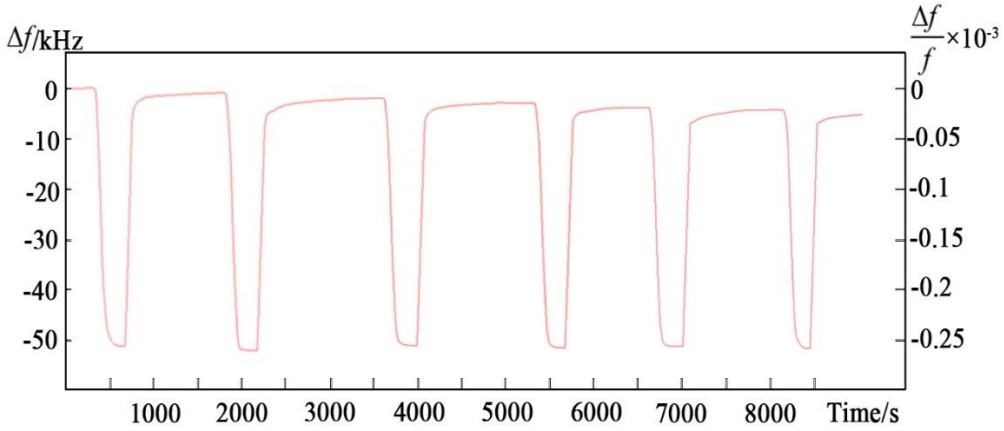
Δf/kHz
Δf/f ×10⁻³
Time/s

(b)

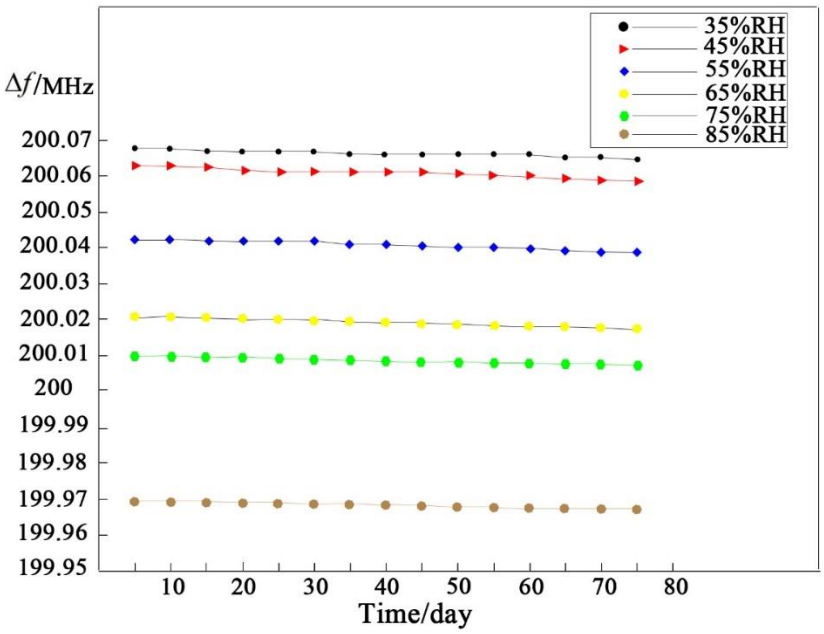

(c)

Fig.10. (a) Relationship between temperature and frequency shifts; (b) Frequency changes of the SAW devices when the RH is changed from 35%RH to 65%RH, repeated six times in a short period of time; (c) The SAW sensor coated with SA film was placed under six different RHs (35% RH, 45% RH, 55% RH, 65% RH, 75% RH, 85% RH) for 75 days.